Modeling of resistive wall mode and its control in experiments and ITER

Yueqiang Liu, M. S. Chu, A. M. Garofalo, R. J. La Haye, Y. Gribov, M. Gryaznevich, T. C. Hender, D. F. Howell, P. de Vries, M. Okabayashi, S. D. Pinches, H. Reimerdes, and EFDA-JET contributors

---

Articles you may be interested in

Feedback stabilization of nonaxisymmetric resistive wall modes in tokamaks. I. Electromagnetic model
Physics of Plasmas **7**, 3681 (2000); 10.1063/1.1287744

Kinetic damping of resistive wall modes in ITER
Physics of Plasmas **19**, 052502 (2012); 10.1063/1.4714877

Toroidal self-consistent modeling of drift kinetic effects on the resistive wall mode
Physics of Plasmas **15**, 112503 (2008); 10.1063/1.3008045

The role of kinetic effects, including plasma rotation and energetic particles, in resistive wall mode stability
Physics of Plasmas **17**, 082504 (2010); 10.1063/1.3474925

Magnetic control of magnetohydrodynamic instabilities in tokamaks
Physics of Plasmas **22**, 021803 (2015); 10.1063/1.4902126

Magnetic drift kinetic damping of the resistive wall mode in large aspect ratio tokamaks
Physics of Plasmas **15**, 092505 (2008); 10.1063/1.2978091

Modeling of resistive wall mode and its control in experiments and ITER[a]

Yueqiang Liu[b]
Department of Applied Mechanics, EURATOM/VR Fusion Association, Chalmers University of Technology, Göteborg, Sweden S-41296

M. S. Chu, A. M. Garofalo, and R. J. La Haye
General Atomics, San Diego, California 92186–5608

Y. Gribov
Physics Unit, ITER Naka Joint Work Site, Naka, Ibaraki, Japan 311–0193

M. Gryaznevich, T. C. Hender, D. F. Howell, and P. de Vries
Euratom/UKAEA Fusion Association, Culham Science Centre, Abingdon, Oxon, OX14 3DB, United Kingdom

M. Okabayashi
Princeton Plasma Physics Laboratory, Princeton, New Jersey 08543

S. D. Pinches
Max-Planck-Institute for Plasmaphysik, EURATOM-Association, Garching, Germany D-85748

H. Reimerdes
Columbia University, New York, New York 10027

EFDA-JET contributors[c]

Active control of the resistive wall mode (RWM) for DIII-D [Luxon and Davis, Fusion Technol. **8**, 441 (1985)] plasmas is studied using the MARS-F code [Y. Q. Liu, *et al.*, Phys. Plasmas **7**, 3681 (2000)]. Control optimization shows that the mode can be stabilized up to the ideal wall beta limit, using the internal control coils (I-coils) and poloidal sensors located at the outboard midplane, in combination with an ideal amplifier. With the present DIII-D power supply model, the stabilization is achieved up to 70% of the range between no-wall and ideal-wall limits. Reasonably good quantitative agreement is achieved between MARS-F simulations and experiments on DIII-D and JET (Joint European Torus) [P. H. Rebut *et al.*, Nucl. Fusion **25**, 1011 (1985)] on critical rotation for the mode stabilization. Dynamics of rotationally stabilized plasmas is well described by a *single* mode approximation; whilst a strongly unstable plasma requires a *multiple* mode description. For ITER [R. Aymar, P. Barabaschi, and Y. Shimomura, Plasma Phys. Controlled Fusion **44**, 519 (2002)], the MARS-F simulations show the plasma rotation may not provide a robust mechanism for the RWM stabilization in the advanced scenario. With the assumption of ideal amplifiers, and using optimally tuned controllers and sensor signals, the present feedback coil design in ITER allows stabilization of the $n=1$ RWM for plasma pressures up to 80% of the range between the no-wall and ideal-wall limits. © *2006 American Institute of Physics*. [DOI: 10.1063/1.2177199]

I. INTRODUCTION

Advanced tokamaks are economically attractive fusion devices, which aim at steady state operation with a high plasma pressure and a large fraction of bootstrap current.[1] One of the good features of advanced tokamaks is that the microinstabilities in the plasma core region are well damped, which leads to internal transport barriers, and thus improved plasma energy confinement. Moreover, it is expected that in advanced scenarios with low or reversed magnetic shear, neoclassical tearing modes, that are a very dangerous magnetohydrodynamic (MHD) instabilities for long pulse opera-

tions for present tokamaks and possibly for ITER, can actually be suppressed. On the other hand, it is known that the product of the plasma pressure, $\beta = 2\mu_0\langle p\rangle/\langle B^2\rangle$, and the bootstrap current fraction, $f_{bs} = I_{bs}/I_p$, (where p is the plasma kinetic pressure, B the total magnetic field, $\langle \cdots \rangle$ defined as the average over plasma volume, I_{bs} the bootstrap current, I_p total plasma current) has an upper limit[2]

$$\beta f_{bs} < 0.1(1 + \kappa^2)(a/R)^{1/2}\beta_N^2,$$

where $\beta_N = \beta(\%)a(\mathrm{m})B_0(\mathrm{T})/I_p(\mathrm{MA})$ is the normalized beta. For advanced scenarios such as the ITER Scenario-4,[3] with conventional plasma aspect ratio $R/a \simeq 3$, and moderate plasma elongation $\kappa < 2$, improvement of the fusion performance requires maximizing β_N. However, rather broad current profiles and highly peaked pressures, typical for advanced plasmas, lead to relatively low pressure limits due to

the instability of long-wavelength (low toroidal mode number n) ideal MHD kink modes. These pressure-driven, external kink instabilities can in principle be suppressed by a closely fitted conducting wall surrounding the plasma. In practice, however, walls have finite resistivity. On the time scale over which eddy currents in the wall decay resistively, the magnetic perturbations of external modes penetrate the wall, and the stabilization is lost.[4] The resulting slow-growing, resistive wall modes (RWM) need to be stabilized to achieve high β_N in steady state operations. It is predicted that, for the ITER advanced scenario, β_N can be increased from about 2.5 up to 3.5 or even more, provided the $n=1$ RWM is stabilized.[5]

Two possible ways have been suggested to stabilize the low n RWM in a tokamak. The simple way is to rely passively on the plasma rotation. Both toroidal theory[6,7] and experiments in DIII-D (Refs. 8–10) and JET (Joint European Torus) (Ref. 11) show that a high-speed toroidal rotation, typically a few percent of the Alfvén speed at the plasma center, is required for complete stabilization of the mode. One of the key physics issues is understanding of the damping mechanisms on the RWM due to the nonlinear interaction between the mode and the (stable) waves and particles in the plasma.

Another way, first proposed by Bishop,[12] exploits active control. This technique is similar to the routinely used vertical control for elongated plasmas.[13] Feedback control of the RWM has been carried out in DIII-D,[14–18] HBT-EP (High Beta Tokamak-Extended Pulse),[19] as well as in EXTRAP T2R reversed field pinch,[20,21] with very encouraging results. Theoretically, a circuit model,[22] cylindrical models,[23–27] and toroidal models[28–33] have been developed to study feedback stabilization of the RWM. One of the key understandings is that sensors, measuring the poloidal component of the magnetic field perturbations just inside the vacuum vessel, gives superior control performance to sensors measuring the radial fields.[29]

Recent experiments in DIII-D show very efficient stabilization by using internal control coils (I-coils), installed inside the vacuum vessel and above/below the midplane on the large major radius side of the torus.[18] This paper reports the feedback simulation results for DIII-D plasmas using I-coils. Also, a feedback study is made for ITER plasmas in advanced scenarios.

One way to understand the RWM damping is to compare the experimental data with numerical simulations with various damping models. Two types of experimental data are well documented: the critical rotation frequency required for marginal stabilization of the RWM, and the amplitude and phase of the plasma response to an externally applied resonant field [resonant field amplification (RFA), Ref. 34]. This paper reports both types of simulations using the MARS-F code,[29] and compares with experiments in DIII-D and JET.

MARS-F is a linear MHD stability code developed from the MARS code,[35,36] with added features such as feedback[28] and the kinetic damping model.[37] The latter is based on a simplified drift-kinetic large-aspect-ratio analysis.[38] Besides the Alfvén continuum damping, a parallel viscous force[36] is
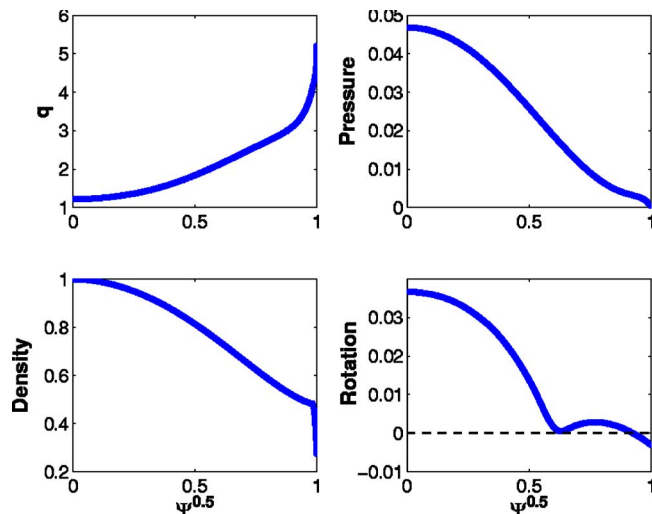

FIG. 1. (Color online) An equilibrium reconstructed from DIII-D shot 114340 at 1450 ms. Shown are the profiles for the safety factor q, plasma pressure (normalized by the toroidal magnetic field pressure), and density (normalized at the plasma center), and the toroidal plasma rotation frequency (normalized by the Alfvén frequency). Ψ is the normalized poloidal magnetic flux.

also introduced in the code in order to model the sound wave damping.

Section II of this paper reports the feedback simulations for DIII-D plasmas using I-coils. Section III gives ITER predictions for active control of the RWM. Section IV compares the MARS-F computed critical rotation with the recent experiments on DIII-D and JET, and gives predictions for ITER. Section V discusses modeling issues of the plasma response for the resonant field amplification. The work is summarized in Sec. VI.

II. FEEDBACK STUDY FOR DIII-D

To simulate the feedback experiments on DIII-D, we choose a plasma equilibrium reconstructed from shot 114340 at 1450 ms. The profiles for the safety factor q, the plasma pressure and density, as well as the plasma toroidal rotation are shown in Fig. 1. For this shot, the plasma rotation is kept very slow in a large outer region of the plasma. The resistive wall mode is *not* stabilized by the plasma rotation. Feedback control, using internal coils (I-coils), keeps the mode stable for more than 50 ms at low rotation.[18]

A. Computing plasma response model

In the simulation, we neglect the plasma rotation. Using the MARS-F code, we compute the plasma response model, defined as a frequency dependent transfer function[39]

$$P = \frac{\psi_s}{M_{sf} I_f}, \tag{1}$$

where ψ_s is the magnetic flux detected by poloidal sensors located at the outboard midplane just inside the DIII-D vacuum vessel. M_{sf} is a normalization factor, chosen as the *radial* field produced at the sensor position by 1 A current flowing in the I-coils in free space. The feedback current is

denoted as I_f. The open-loop response P is usually well approximated by a low order rational function (Padé approximation).[28]

We compute transfer functions P_U and P_L for both sets of I-coils above and below the midplane, respectively. The poloidal sensors at the midplane is used for both sets of I-coils. Assuming the sensor signal is fed back to two sets of I-coils via the same controller K, and with opposite toroidal phase shift $\pm\phi_P$ (the total phasing between the upper and lower coil sets becomes $2\phi_P$), the total transfer function is

$$P = P_U \exp(j\phi_P) + P_L \exp(-j\phi_P), \qquad (2)$$

where j is the imaginary unit.

B. Control optimization

The control optimization is performed, that (1) gives stabilization of the RWM, (2) meets certain prescribed criteria on the control performance. We assume a simple PD-controller with proportional (P) and derivative (D) actions

$$K(s) = K_p \frac{1 + T_d s}{1 + T_d s/\xi}, \qquad (3)$$

where s is the Laplace variable. K_p is the proportional gain, generally chosen as a complex number with phase ϕ_K. (ϕ_K corresponds to a toroidal phase shift between the control signal and the sensor signal.) T_d (real number) is the derivative gain. An additional parameter $\xi > 1$ is chosen to prevent unphysical behavior at very high frequencies. The control performance is measured by control activity $\|KS\|_\infty$ and sensitivity $\|S\|_\infty$ (Ref. 40)

$$S(j\omega) = \frac{1}{1 + K(j\omega)P(j\omega)}, \quad \|KS\|_\infty = \sup_\omega |K(j\omega)S(j\omega)|,$$

$$\|S\|_\infty = \sup_\omega |S(j\omega)|, \qquad (4)$$

where ω is the real frequency belonging to a chosen frequency band. In the control optimization, we minimize the control activity $\|KS\|_\infty$ while applying constraints on the sensitivity $\|S\|_\infty \leq 2.0$. Three strategies are tested with respect to the choice of the optimization variables c: (1) $c=\{K_p, T_d, \xi\}$, where K_p is real (i.e., $\phi_K=0$), fix $\phi_P=150°$; (2) $c=\{K_p, T_d, \xi, \phi_P\}$, fix $\phi_K=0$; (3) $c=\{K_p, T_d, \xi, \phi_P\}$, where K_p is complex (i.e., also optimize ϕ_K).

We perform a control study for both ideal power amplifiers (with zero time delay and infinite bandwidth) and the DIII-D experimental amplifiers.

C. Control with ideal amplifier

Figure 2 shows the control results for a plasma close to the ideal wall limit at $C_\beta \equiv (\beta - \beta^{\text{no-wall}})/(\beta^{\text{ideal-wall}} - \beta^{\text{no-wall}})$ $=0.9$. The instability of the RWM and the possibility of its feedback control is usually well correlated to the parameter C_β. Figures 2(a) and 2(b) show, in the complex plane, the computed transfer function $P_U(j\omega)$ and $P_L(j\omega)$, with real frequencies (normalized by the wall time) $\omega\tau_w \in [-10^3, 10^3]$. Figure 2(c) shows the transfer function $K(j\omega)P(j\omega)$ for the
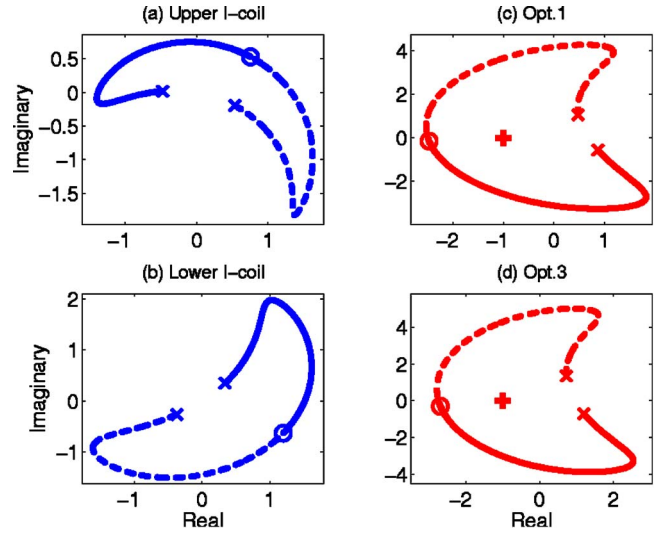

FIG. 2. (Color online) Transfer functions plotted on the complex plane, for real frequencies $-10^3 \leq \omega\tau_w \leq 10^3$. Solid (dashed) line denotes positive (negative) ω. $\bigcirc$ denotes $\omega=0$, and $\times$ denotes $|\omega\tau_w|=10^3$. Shown is a case for the plasma close to the ideal wall beta limit with $C_\beta=0.9$. An ideal amplifier is assumed. (a) Plasma response to the internal control coils (I-coils) above the midplane. (b) Plasma response to the I-coils below the midplane. (c) Plasma response to both sets of I-coils connected to the same optimal PD controller with *real* feedback gains. Toroidal phase difference between upper and lower sets is 300°. (d) Plasma response to both sets of I-coils connected to the same optimal PD controller with *complex* feedback gains. Both toroidal phasings of feedback gains and I-coil sets are also optimized.

optimal controller K according to the optimization strategy (1). The corresponding result for the optimization strategy (3) is shown in Fig. 2(d).

According to the Cauchy principle of phase variation, the closed loop is stable if the Nyquist curves, shown in Fig. 2, encircle -1 once in the counterclockwise direction, as the frequency ω varies from $-\infty$ to $+\infty$. In our case, both closed-loops from Figs. 2(c) and 2(d) are stable, with rather good stability margin. [A quantitative measure of the stability margin is the sensitivity $\|S\|_\infty$. The shortest distance between -1 and the Nyquist curve for $K(j\omega)P(j\omega)$ is equal to $1/\|S\|_\infty$, since according to the definition, $1/\max|S(j\omega)|=\min|1+K(j\omega)P(j\omega)|$.]

The similarity of Figs. 2(c) and 2(d) indicates that the ad hoc choice of $\phi_P=150°$ is close to the optimal, and feedback with real gains is good enough for this case. Indeed, the quantitative measures of the control activity $\|KS\|_\infty$ and sensitivity $\|S\|_\infty$ are quite close, as shown in Fig. 3, for all three optimization strategies. The control optimization is made individually for each C_β value. We conclude also that, with an ideal amplifier, the I-coils can provide full stabilization of the RWM up to the ideal wall beta limit, with good performance.

The optimal controller gains K_p and T_d are shown in Figs. 4(a) and 4(b), respectively. The optimal value for parameter ξ is generally much larger than unity. We note that the derivative action is almost not required. The phase angles ϕ_K and ϕ_P are shown in Figs. 5(a) and 5(b), respectively. The optimal phasing between two sets of I-coils can be as low as 240° at low pressure. The fact that the optimal control
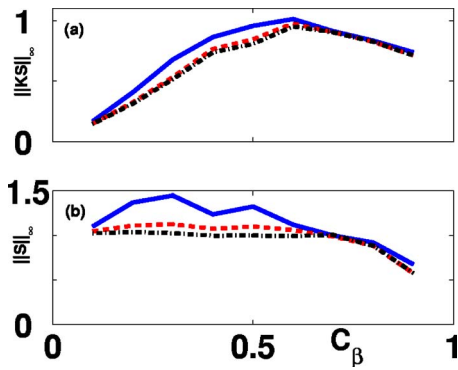
FIG. 3. (Color online) Optimal control results with ideal amplifiers. Solid curves correspond to real feedback gains and fixed toroidal phasing at 300° between upper and lower I-coil sets. Dashed curves correspond to real gains and optimal phasing for I-coils. Dashed-dotted curves correspond to optimal phasing for both complex gains and I-coil sets. Shown are (a) the optimal control activity $\|KS\|_\infty$, and (b) the achieved stability margin $\|S\|_\infty$, vs the plasma pressure C_β. Controller optimization is made for each C_β individually.

FIG. 5. (Color online) The same cases as in Fig. 3. Shown are (a) toroidal phasings (in degrees) for optimal feedback gains, and (b) half of toroidal phasing (in degrees) between upper and lower sets of I-coils.

results are only slightly better than the ad hoc choice of 300° indicates, that the control is not very sensitive to the choice of ϕ_P.

D. Control with DIII-D amplifier

We use the following transfer function to specify the DIII-D switching power amplifiers, which were installed in 2000 (Ref. 41):

$$P_a(s) = \frac{\Omega_1}{s + \Omega_1} \times \frac{\Omega_2}{s + \Omega_2} \times \exp(- s\tau_d), \qquad (5)$$

where $\Omega_1 = 5373 - 8205$ J s^{-1}, $\Omega_2 = 2692 + 960$ J s^{-1}, $\tau_d = 65$ μs.

The total open-loop transfer function $P(s)$ is now replaced by $P(s)P_a(s)$. We perform again the control optimization for all C_β. Figure 6 shows the results for $C_\beta = 0.7$ in Nyquist diagrams. At this plasma pressure, the optimal con-

troller can marginally stabilize the mode, with rather poor performance. No optimal controller is found at $C_\beta = 0.8$ that can still stabilize the mode.

Figure 7 shows the optimal control results for varying plasma pressures. At $C_\beta > 0.3$, the control performance specification $\|S\|_\infty \leq 2.0$ can no longer be satisfied, as shown in Fig. 7(b).

The optimal control gains are shown in Figs. 8(a) and 8(b). Larger derivative gains (about 10% of the proportional gain) are generally required in order to compensate the phase delay caused by the power supply. The optimal phase angles for ϕ_K and ϕ_P varies with varying plasma pressure (Fig. 9), which does not lead to significant variation of the control results.
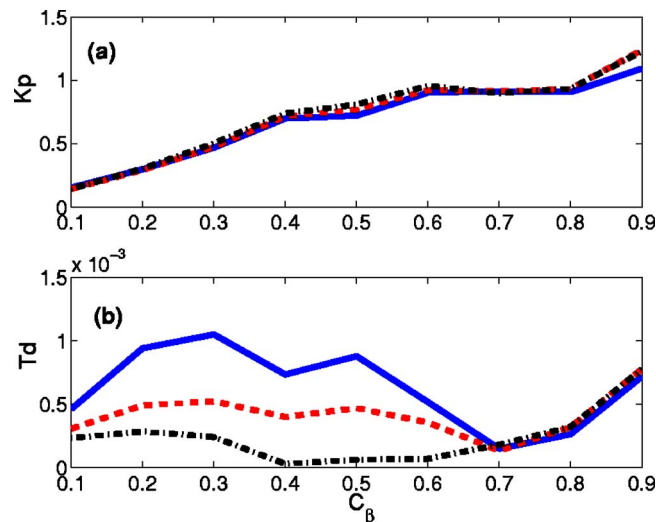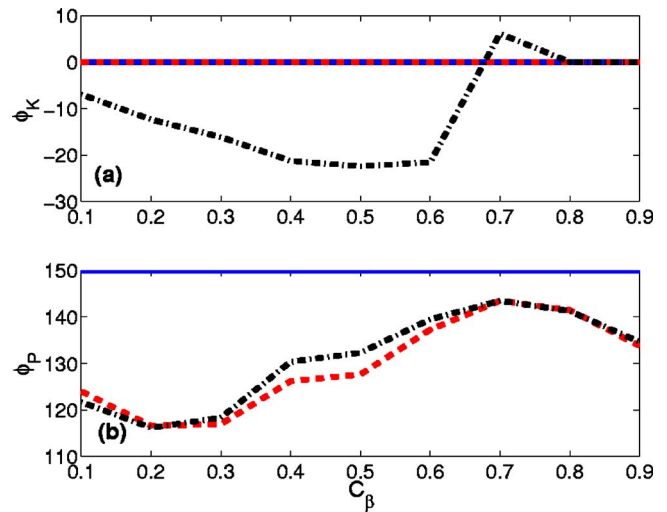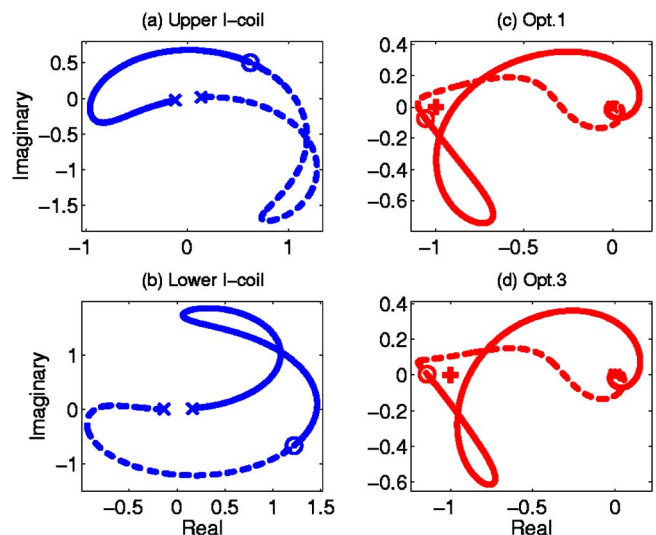

FIG. 4. (Color online) The same cases as in Fig. 3. Shown are optimal controller gains (amplitude) for (a) proportional action K_p, and (b) derivative action T_d.

FIG. 6. (Color online) A similar study to Fig. 2, with the plasma pressure at $C_\beta = 0.7$. A realistic power supply model from DIII-D experiments is included in the control optimization.
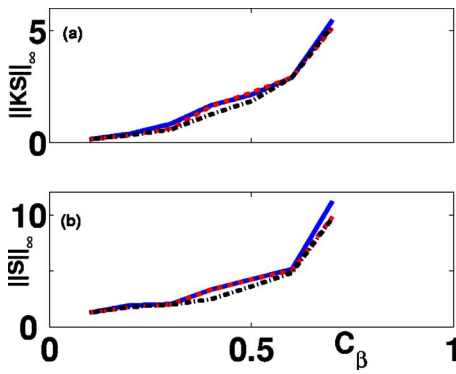
FIG. 7. (Color online) Optimal control results with the DIII-D amplifier. The curves notation follows Fig. 3.

III. FEEDBACK STUDY FOR ITER

We also studied active control of the $n=1$ RWM for the ITER steady state scenario (Scenario-4).[3,5] This scenario has weak negative magnetic shear and a highly shaped plasma. The total plasma current is 9 MA, with about 340 MW fusion power production at $Q=5$. The design plasma is marginally unstable without the wall. We scaled the plasma pressure up to the ideal-wall limit for the inner wall, keeping the total plasma current at 9 MA.

The side correction coils have been used for the RWM feedback control. These are superconducting coils, located along the outboard midplane and external to the ITER walls (at a radial distance of about $3a$, where a the plasma minor radius), with three pairs of toroidally opposite coils connected to produce the $n=1$ magnetic field.

Using internal poloidal sensors and assuming an ideal amplifier, MARS-F calculations have shown that the present design of feedback coils allow stabilization of the $n=1$ RWM up to $C_\beta \simeq 60\%$ with proportional actions alone. Better results can be achieved by using optimally tuned proportional, integral, and derivative (PID) controllers and improved sensor signals. We have optimized the PID gains to
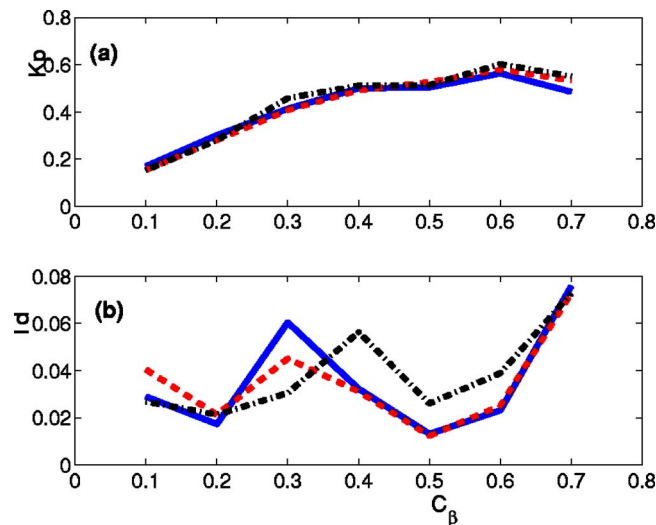

FIG. 8. (Color online) Optimal controller obtained assuming the DIII-D amplifier. Notations are the same as in Fig. 4.
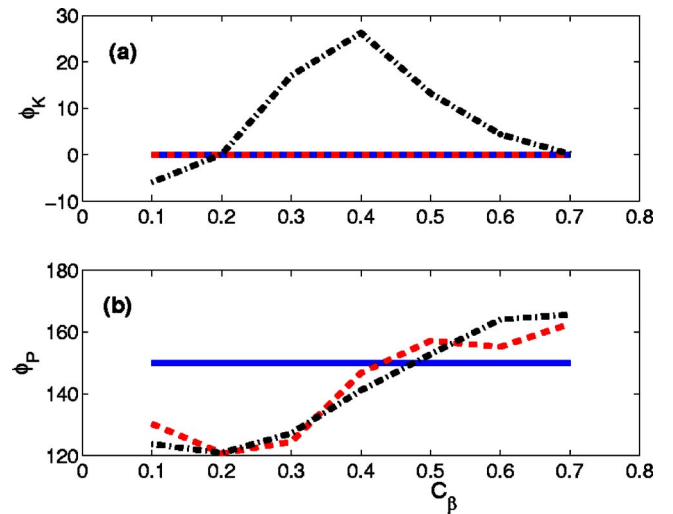

FIG. 9. (Color online) Optimal toroidal phasings assuming the DIII-D amplifier. Notations are the same as in Fig. 5.

achieve the minimum peak voltage for a reference event, where the controller is turned on after the field reaches 1.5 mT.

In Ref. 37, we have shown that, with the design voltage limit of 300 V/turn for the amplifier, the RWM can be controlled with good performance ($\|S\|_\infty = 2$) for $C_\beta \lesssim 65\%$, and with moderate performance ($\|S\|_\infty = 2.5$) for $C_\beta \lesssim 70\%$. The peak voltage is further reduced if we use internal poloidal sensor signals compensated by an optimally chosen signal. The RWM can be stabilized, with good performance, up to $C_\beta \gtrsim 80\%$.

IV. CRITICAL ROTATION FOR RWM STABILIZATION

A. Simulations for DIII-D

On DIII-D, the critical rotation, required for stabilization of the RWM, is measured by applying an external error magnetic field to gradually slow the plasma rotation. One example is shot 121611, which is part of a DIII-D/JET comparison of RWM physics.[42] Figure 10 shows the equilibrium profiles reconstructed at high beta shortly before the onset of the RWM. The rotation profile (normalized at the plasma center) at this moment is shown as a solid line. Shown also is the rotation profile measured before applying the external field (dashed line), when the plasma is stabilized by the rotation.

The MARS-F computed critical rotation (evaluated at the plasma center) is shown in Fig. 11, for both rotation profiles. The kinetic damping model is assumed. The computed critical rotation with magnetic braking (profile 2) is close to the experimental value, as shown by the solid line. The computed critical rotation at the plasma center is reduced by about 40% for the case without magnetic braking (profile 1). This comparison shows that the critical rotation, as defined at the plasma center, is sensitive to the rotation profile.

We also compute the critical rotation for the equilibrium that was used in the feedback study described in Sec. II. The equilibrium and rotation profiles are shown in Fig. 1. In Fig.
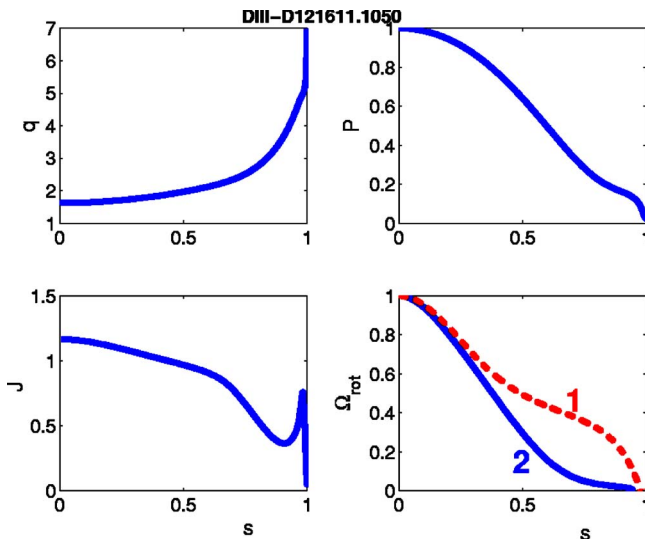
FIG. 10. (Color online) Equilibrium profiles reconstructed for the DIII-D shot 121611 at 1165.5 ms, for the safety factor q, plasma pressure P (normalized at the plasma center), and surface averaged current density J [normalized by $B_0/(\mu_0 R_0)$, where B_0 is the toroidal vacuum field, R_0 is the major radius, and μ_0 is the vacuum permeability], and toroidal rotation Ω_{rot} (normalized at the plasma center). Two rotation profiles are considered: before applying the external field (dashed curve) and after the magnetic braking (solid curve), when the critical rotation is measured.

FIG. 12. (Color online) Computed critical rotation versus the plasma pressure C_β for the DIII-D shot 114340. The equilibrium and rotation profiles are shown in Fig. 1.

12, we plot the ratio of the computed critical rotation to the experimental value, for increasing plasma pressures. The plasma pressure in the experiment corresponds to C_β about 0.35. The RWM at this pressure is predicted to be unstable, which confirms the experimental observations.

B. Simulations for JET

Figure 13 shows comparison of the MARS-F computed critical rotation against the experimental data on JET. The calculations assume either parallel sound wave damping (dashed curves), with various values for adjustable damping
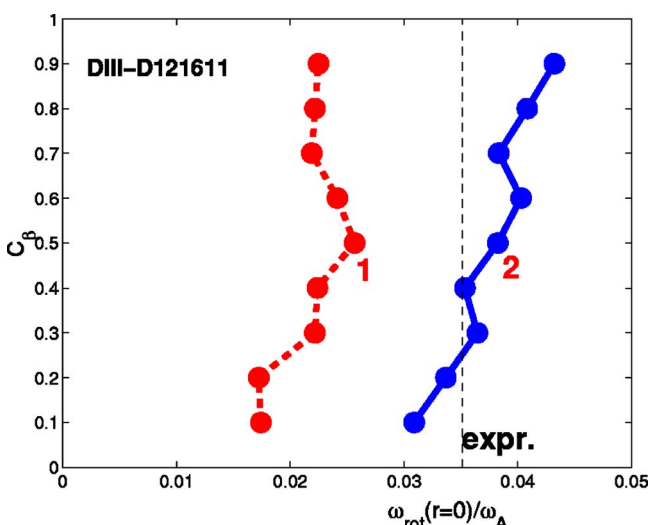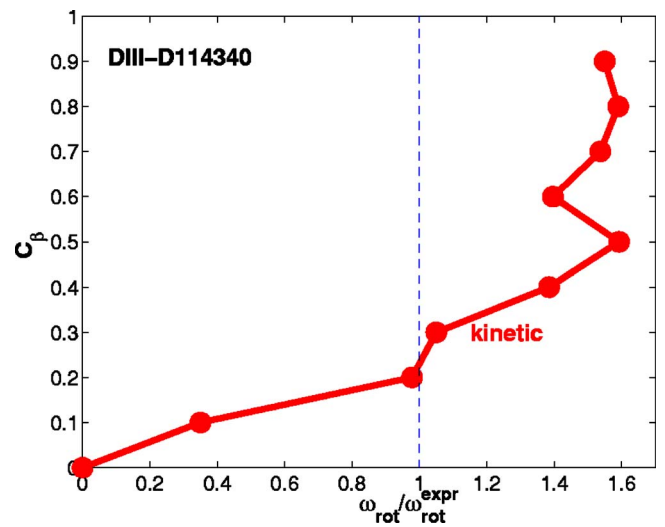
coefficient $\kappa_\parallel$, or the kinetic damping (solid curve). A series of JET equilibria, reconstructed from JET shot 62366, has been used in calculations.[37] The kinetic damping gives quantitatively correct predictions for the critical rotation.

C. The q_{95} scaling

Using the kinetic damping model, it has been computed in Ref. 37, that the critical rotation, measured at the plasma center, decreases with increasing q_{95}. The dependence follows an approximate scaling as $1/q_{95}^2$ as shown in Fig. 14. In the same figure, we also plot the critical rotation at the $q=2$ surface versus q_{95}. No explicit dependence is seen. Both observations are also made in experiments in DIII-D, JET, and NSTX.[42] One possible explanation for this is the variation of rotation profiles between different machines, as

FIG. 11. (Color online) Computed critical rotation versus the plasma pressure C_β, for both rotation profiles shown in Fig. 10. The kinetic damping model is used in MARS-F calculations. Shown also the critical rotation measured in the magnetic braking experiment.
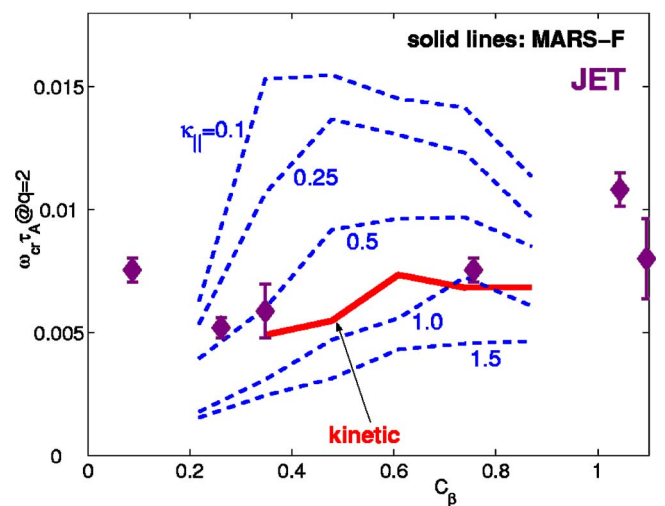

FIG. 13. (Color online) The critical rotation frequency at the $q=2$ surface, normalized by Alfvén frequency, versus the plasma pressure C_β. Plotted are JET experimental data (dots) and the MARS-F results with parallel sound wave damping (dashed curves) and semikinetic damping (solid curve) models.
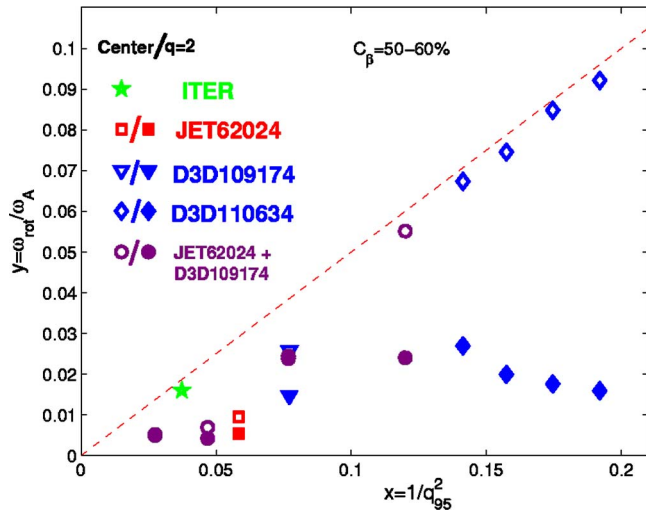
FIG. 14. (Color online) The q_{95} scan of the *computed* critical rotation frequency ω_{rot}, normalized by the Alfvén frequency ω_A, for various equilibria. The plasma pressure is kept approximately the same in terms of $C_\beta(=50\% - 60\%)$. The critical rotation frequencies are defined both at the plasma center (open symbols) and at the $q=2$ surface (filled symbol).

shown in Fig. 15. [For a similar q-profile from two machines and a similar critical rotation at the $q=2$ surface, a more strongly peaked rotation profile (in DIII-D as compared to JET, for example) could give a larger critical rotation evaluated at the plasma center.] Even with a fixed rotation profile, the dependence can be different for the critical rotation at the plasma center compared with that at the $q=2$ surface, as shown by the computed data for DIII-D 110634 in Fig. 14. This is because increasing q_{95} shifts the $q=2$ surface inward into the plasma, where the rotation speed is higher.

Figure 14 also shows the critical rotation predicted for the ITER advanced plasmas from Scenario-4. Transport calculations in Ref. 3 indicate that the ITER plasma rotation speed is close to the MARS-F computed critical value (less
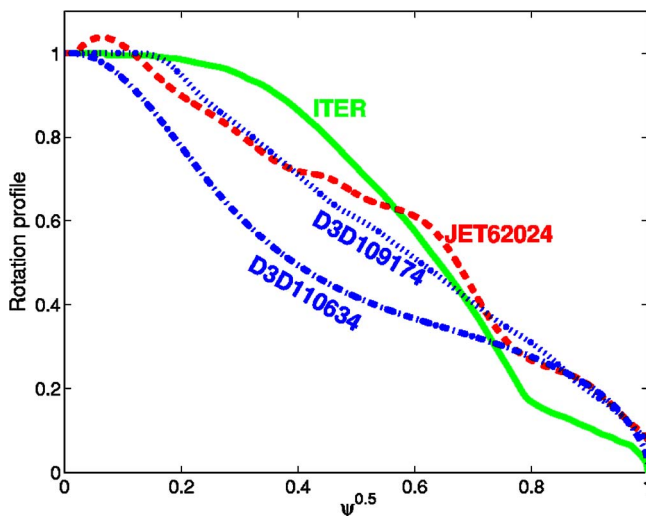

FIG. 15. (Color online) The rotation profiles (normalized by the central value) used in the calculations in Fig. 14 for various equilibria. The rotation profile for ITER is predicted by transport calculations (Ref. 3).
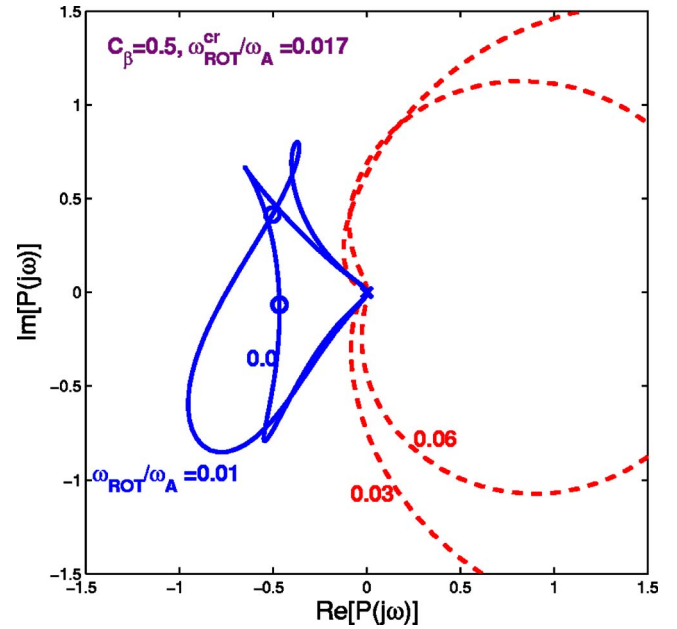

FIG. 16. (Color online) Nyquist plot of transfer functions for both unstable (solid curves) and stable (dashed curves) plasma response. A test toroidal equilibrium with JET-like shape and $C_\beta=0.5$ is considered. The RWM is unstable at low plasma rotation and eventually stabilized by a rotation frequency larger than $0.017\omega_A$ at the plasma center.

than 2% of the Alfvén speed at the plasma center). Therefore, ITER plasma rotation may not provide a robust stabilization mechanism for the RWM.

V. DYNAMICS OF STABLE RWM

The transfer function, defined in Eq. (1), can also be used to describe the dynamics of a stable plasma, where the RWM is stabilized by fast plasma rotation. The current I_f produces a resonant error field, that can be amplified by the stable plasma.[34] We try to establish how many poles (modes) are required to adequately represent the plasma response.

We choose a test toroidal equilibrium with the JET-like shape, and compute the plasma response with various rotation speeds. The RWM for the chosen equilibrium (with the plasma pressure β_N at the middle between the no-wall and the ideal-wall limits) is stabilized by a critical rotation $\omega_{rot}^{cr}/\omega_A=0.017$ at the plasma center. Figure 16 shows the Nyquist plot for the plasma response for four rotation speeds: $\omega_{rot}/\omega_A=0.0,0.01,0.03,0.06$. In the first two cases (solid curves), the plasma is *unstable*. A minimum of 3 poles are required to reach a good approximation of the plasma response computed by the MARS-F. The Nyquist curves for the last two cases (dashed), where the plasma is *stable*, are very close to circles. Such a response is well described by a single pole transfer function.

As an example, the plasma response at $\omega_{rot}/\omega_A=0.01$ is well approximated by a transfer function
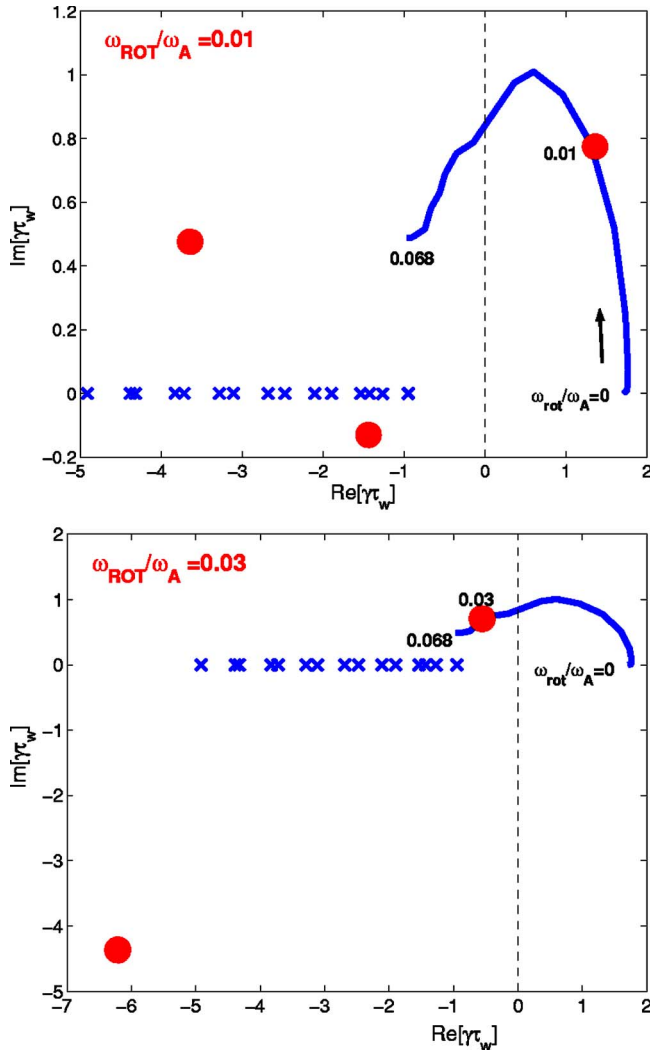
FIG. 17. (Color online) Poles (●) in the rational function approximation for the *unstable (stable)* plasma response at plasma rotation ω_{rot}/ω_A =0.01(0.03). As for a reference, also shown are growth rates (solid lines) of the unstable RWM with increasing rotation frequency, as well as damping rates (×) of the stable RWM at no rotation.

$$P(s) = \frac{1.5046 + 0.1124j}{s - 1.3586 - 0.7745j} + \frac{1.3205 + 0.4451j}{s + 1.4399 + 0.1298j}$$
$$+ \frac{-2.1849 - 0.5422j}{s + 3.6456 - 0.4760j}. \qquad (6)$$

Figure 17(a) shows the three poles in the complex plane, together with the growth rates (●) of the unstable RWM with increasing the rotation frequency, as well as the damping rates (×) of the stable RWM at no rotation. The unstable pole coincides with the growth rate of the unstable RWM. The two stable poles lump the contribution from all the stable RWMs. Note that these two stable poles are located close to the origin, giving a significant contribution to the total plasma response.

At ω_{rot}/ω_A=0.03, the plasma is stable. We obtain the following function by including two poles

$$P(s) = \frac{1.8283 - 0.1822j}{s + 0.5530 - 0.7080j} + \frac{-1.2261 - 0.4807j}{s + 6.2110 + 4.3657j}. \qquad (7)$$

The poles are plotted in Fig. 17(b), together with the growth/damping rates of the RWM computed by MARS-F. Note that the first stable pole corresponds to the damping rate of the RWM stabilized by the plasma rotation. The second, lumped pole is rather far from the origin, giving a minor contribution to the total plasma response. (The contribution from the second pole becomes significant only at higher frequencies out of the frequency range for the RWM.) Therefore, we conclude that a single pole can give a good approximation for the response of stable plasmas. This explains why a single mode model works well in interpreting the experimental data from the RFA experiments.[43]

VI. CONCLUSIONS AND DISCUSSIONS

Using the MARS-F code, feedback stabilization of the RWM is simulated for DIII-D plasmas. Control optimization has been performed based on the computed plasma response models. The DIII-D I-coils, with outboard midplane internal poloidal sensors and *ideal amplifiers*, can provide stabilization of the RWM up to the ideal wall beta limit. With the *DIII-D switching power amplifiers*, the stabilization up to C_β=0.7 can be achieved.

Reasonably good quantitative agreement is achieved between MARS-F simulations and experiments on DIII-D and JET, on the critical rotation for the mode stabilization. The computed q_{95} scaling is also confirmed by the experimental measurements. The kinetic damping model is an essential ingredient for achieving the agreement. Calculations for DIII-D plasmas also show that the critical rotation is sensitive to the rotation profile.

Dynamics of rotationally stabilized plasmas, the so-called resonant field amplification, is well described by a *single* mode approximation; whilst a strongly unstable plasma requires a *multiple* mode description.

According to the kinetic damping model, the ITER plasma rotation is close to the predicted critical value, and thus may not provide a robust mechanism for the RWM stabilization in the advanced Scenario-4. Active control of the mode using feedback is an alternative way to stabilize the RWM in ITER.

With the present feedback coil design for ITER, it is possible to stabilize the n=1 RWM for plasma pressures up to C_β=0.8, using optimally tuned PID controllers and optimally compensated internal poloidal sensor signals.

For more realistic prediction of the feedback performance in ITER, other issues such as 3D wall effects, system noise and the superconducting coil ac losses, need to be addressed.

[1] C. Kessel, J. Manickam, G. Rewoldt, and W. M. Tang, Phys. Rev. Lett. **72**, 1212 (1994).

[2] A. Bondeson, D. H. Liu, F. X. Söldner, M. Persson, Yu. F. Baranov, and G. T. A. Huysmans, Nucl. Fusion **39**, 1523 (1999).

[3] A. Polevoi, S. Yu. Medvedev, V. D. Pustovitov, V. S. Mukhovatov, M. Shimada, A. A. Ivanov, Yu. Yu. Poshekhonov, and M. S. Chu, Fusion Energy, in Proceedings of the 19th International Conference, Lyon, 2002 (IAEA, Vienna, 2002), CD-ROM file CT/P-08 and http://www.iaea.org/programmes/ripc/physics/fec2002/html/fec2002.htm

[4] D. Pfirsch and H. Tasso, Nucl. Fusion **11**, 259 (1971).

[5] Y. Q. Liu, A. Bondeson, Y. Gribov, and A. Polevoi, Nucl. Fusion **44**, 232 (2004).

[6] A. Bondeson and D. J. Ward, Phys. Rev. Lett. **72**, 2709 (1994).

[7] D. Gregoratto, A. Bondeson, M. S. Chu, and A. M. Garofalo, Plasma Phys. Controlled Fusion **43**, 1425 (2001).

[8] A. M. Garofalo, A. D. Turnbull, M. E. Austin et al., Phys. Rev. Lett. **82**, 3811 (1999).

[9] A. M. Garofalo, T. H. Jensen, L. C. Johnson et al., Phys. Plasmas **9**, 1997 (2002).

[10] R. J. La Haye, A. Bondeson, M. S. Chu, A. M. Garofalo, Y. Q. Liu, G. A. Navratil, M. Okabayashi, H. Reimerdes, and E. J. Strait, Nucl. Fusion **44**, 1197 (2004).

[11] T. C. Hender, M. Gryaznevich, Y. Q. Liu et al., Fusion Energy, in Proceedings of the 20th International Conference, Vilamoura, 2004 (IAEA, Vienna, 2004), CD-ROM file EX/P2–22 and http://www-naweb.iaea.org/napc/physics/fec/fec2004/datasets/index.html

[12] C. M. Bishop, Plasma Phys. Controlled Fusion **31**, 1179 (1989).

[13] E. A. Lazarus, J. B. Lister, and G. H. Neilson, Nucl. Fusion **30**, 111 (1990).

[14] E. D. Fredrickson, J. Bialek, A. M. Garofalo et al., Plasma Phys. Controlled Fusion **43**, 313 (2001).

[15] A. M. Garofalo, M. S. Chu, E. D. Fredrickson et al., Nucl. Fusion **41**, 1171 (2001).

[16] M. Okabayashi, J. Bialek, M. S. Chance et al., Phys. Plasmas **8**, 2071 (2001).

[17] E. J. Strait, J. Bialek, N. Bogatu et al., Nucl. Fusion **43**, 430 (2003).

[18] E. J. Strait, J. M. Bialek, I. N. Bogatu et al., Phys. Plasmas **11**, 2505 (2004).

[19] C. Cates, M. Shilov, M. E. Mauel, G. A. Navratil, D. Maurer, S. Mukherjee, D. Nadle, J. Bialek, and A. Boozer, Phys. Plasmas **7**, 3133 (2000).

[20] P. R. Brunsell, D. Yadikin, D. Gregoratto et al., Phys. Rev. Lett. **93**, 225001 (2004).

[21] J. R. Drake, P. R. Brunsell, D. Yadikin et al., Nucl. Fusion **45**, 557 (2005).

[22] M. Okabayashi, N. Pomphrey, and R. E. Hatcher, Nucl. Fusion **38**, 1607 (1998).

[23] R. Fitzpatrick and T. H. Jensen, Phys. Plasmas **3**, 2641 (1996).

[24] V. D. Pustovitov, Plasma Phys. Rep. **27**, 195 (2001).

[25] A. Bondeson, Y. Q. Liu, D. Gregoratto, Y. Gribov, and V. D. Pustovitov, Nucl. Fusion **42**, 768 (2002).

[26] J. M. Finn, Phys. Plasmas **11**, 4361 (2004).

[27] A. H. Boozer, Phys. Plasmas **11**, 110 (2004).

[28] Y. Q. Liu and A. Bondeson, Phys. Rev. Lett. **84**, 907 (2000).

[29] Y. Q. Liu, A. Bondeson, C. M. Fransson, B. Lennartson, and C. Breitholtz, Phys. Plasmas **7**, 3681 (2000).

[30] J. Bialek, A. H. Boozer, M. E. Mauel, and G. A. Navratil, Phys. Plasmas **8**, 2170 (2001).

[31] M. S. Chu, M. S. Chance, A. H. Glasser, and M. Okabayashi, Nucl. Fusion **43**, 441 (2003).

[32] S. Yu. Medvedev and V. D. Pustovitov, Plasma Phys. Rep. **30**, 895 (2004).

[33] Y. Q. Liu, A. Bondeson, D. Gregoratto, C. M. Fransson, Y. Gribov, and R. Paccagnella, Nucl. Fusion **44**, 77 (2004).

[34] A. H. Boozer, Phys. Rev. Lett. **86**, 5059 (2001).

[35] A. Bondeson, G. Vlad, and H. Lütjens, Phys. Fluids B **4**, 1889 (1992).

[36] M. S. Chu, J. M. Greene, T. H. Jensen, R. L. Miller, A. Bondeson, R. W. Johnson, and M. E. Mauel, Phys. Plasmas **2**, 2236 (1995).

[37] Y. Q. Liu, A. Bondeson, M. S. Chu, J-Y. Favez, Y. Gribov, M. Gryaznevich, T. C. Hender, D. F. Howell, R. J. La Haye, and J. B. Lister, Nucl. Fusion **45**, 1131 (2005).

[38] A. Bondeson and M. S. Chu, Phys. Plasmas **3**, 3013 (1996).

[39] A. Bondeson, Y. Q. Liu, D. Gregoratto, C. M. Fransson, B. Lennartson, C. Breitholtz, Y. Gribov, and V. D. Pustovitov, Phys. Plasmas **9**, 2044 (2002).

[40] C. M. Fransson, B. Lennartson, C. Breitholtz, A. Bondeson, and Y. Q. Liu, Phys. Plasmas **7**, 4143 (2000).

[41] A. M. Garofalo, T. H. Jensen, and E. J. Strait, Phys. Plasmas **9**, 4573 (2002).

[42] H. Reimerdes, T. C. Hender, D. F. Howell et al., "Cross-machine comparison of resonant field amplification and resistive wall mode stabilization by plasma rotation," Phys. Plasmas, accepted (2006).

[43] H. Reimerdes, M. S. Chu, A. M. Garofalo, G. L. Jackson, R. J. La Haye, G. A. Navratil, M. Okabayashi, J. T. Scoville, and E. J. Strait, Phys. Rev. Lett. **93**, 135002 (2004).